Journal of Ovonic Research Vol. 9, No. 6, November - December 2013, p. 157 - 165

# CdS QUANTUM DOTS SENSITIZED SINGLE-CRYSTALLINE TiO2 NANOWIRE ARRAY FILMS: PHOTOVOLTAIC PERFORMANCE AND PHOTOELECTRON TRANSPORT PROPERTIES

M LI[*a,b], F-Y SHAO[a], Q-Q BAN[a], J-W YANG[a,b]
[a]*Guangxi Higher Educational Key Laboratory for Novel Technology of Applied Electrochemistry, College of Chemical and Biologic Engineering, Guilin University of Technology, 12 Jiangan Road, Guilin 541004, China*
[b]*Guangxi Provincial Key Lab of New Energy and Building Energy Saving, College of Civil Engineering and Architecture, Guilin University of Technology, 12 Jiangan Road, Guilin 541004, China*

Single-crystalline rutile $TiO_2$ nanowires were synthesized in situ on transparent conductive oxide (TCO) glass substrate and CdS quantum dots (QDs) were deposited on nanowires to form a $TiO_2$/CdS heterojunction structure. The orientation growth, single-crystalline structure of $TiO_2$ nanowire and the core-shell structure of $TiO_2$/CdS were confirmed by XRD, SAED and HR-TEM measurements. The QD sensitized solar cells (QD-SSCs) were assembled and the optical, photoelectrical properties of QD-SSCs were investigated. The results showed that CdS QDs enhanced the optical absorbance of $TiO_2$ in the visible region, therefore greatly improved the photovoltaic performance of solar cells. Under optimum parameters, a power conversion efficiency of 1.72% was achieved. Electron impedance spectroscopy measurement was also carried out to investigate the kinetics of charge transfer and recombination in QD-SSCs. The effects of amount of QDs and photoelectron transport properties of QD-SSCs on the cell efficiency were analyzed. It was proved that the amount of QDs was more important factor than electron lifetime and transfer rate for cell efficiency when the coverage of QDs on $TiO_2$ was not high enough.

(Received August 10, 2013; Accepted October 30, 2013)

*Keywords*: CdS quantum dot; $TiO_2$ nanowire; QD-SSC; Photovoltaic performance; Photoelectron transport property.

## 1. Introduction

Linear $TiO_2$ nanostructure[1-3], such as nanowires, nanotubes have been widely used in solar cells because they provide a type of architecture that could offer a direct and efficient pathway for rapid electron-hole separation and charge transport in contrast to the disordered electron pathway in nanoparticles, as well as high surface areas for interfacial charge transfer and electrochemical reaction[4,5]. Because the grain boundaries can scatter or trap electrons[6], the single-crystalline materials are preferred over polycrystalline ones when used in solar cells.

Semiconductor quantum dots (QDs) have aroused considerable interest in the last years because of their extraordinary physical properties, such as band gap tunability by size control[7], high dipole moments[8] and intrinsic high extinction coefficients[9], which suggest that semiconductor QDs are promising materials as light absorbers. Narrow band gap inorganic semiconducting quantum dot materials including CdS[10,11], PbS[12,13], CdSe[14,15], InP[16], InAs[17] have been explored to serve as photosensitizers in solar cells. The advantages of QD sensitizers over conventional dyes are their adjustable properties to match the solar spectrum better and the

* Corresponding author: liming9989@163.com

ability to generate multiple electron-hole pairs per photon[18]. The *in situ* growth of QDs onto metal oxide matrix is an efficient strategy to obtain a uniform deposition of QD sensitizers on the nanostructure n-type materials. There are different techniques to realize *in situ* growth of QDs, such as chemical bath deposition (CBD) [19,20], electrodeposition[21,22], chemical vapor deposition[23] and sonochemical method[24]. Among them, CBD can guarantee the higher coverage of QDs on the porous materials. Besides, it is a simpler and cheaper method.

In this work, the single-crystalline rutile $TiO_2$ nanowire array (NWA) was synthesized directly on transparent conductive oxide (TCO) glass substrate via hydrothermal method and CBD method was employed to assemble the CdS QDs onto single-crystalline $TiO_2$ nanowires to obtain a core-shell structured. CdS QDs-sensitized solar cells (QD-SSCs) were assembled. The effect of amount of CdS QDs on the photovoltaic performance, the kinetics of charge transfer and recombination of the solar cells were both investigated.

## 2. Experimental

### 2.1 Synthesis of $TiO_2$ nanowire arrays

The hydrothermal method was used to synthesized $TiO_2$ NWA in this work as previously described[25]. All the chemical reagents were analytical grade purity without further purification. 15 ml hydrochloric acid (37 wt%) was mixed with 15ml distilled water in a Teflon-lined stainless steel autoclave followed by stirring at ambient condition. After the addition of 0.5 ml titanium butoxide, the solution was stirred for 5 min. One piece of TCO substrate (14 Ω/□, Nippon Sheet Glass), ultrasonically cleaned in water and ethanol previously, was placed at an angle against the wall of the Teflon reactor with the conductive side facing down. The hydrothermal synthesis was conducted at 150 ℃ for 14 h. After cooling, the TCO substrate was taken out, rinsed extensively with distilled water and dried in air.

### 2.2 Fabrication of CdS sensitized solar cells

The CdS-modified $TiO_2$ NWA films were prepared by CBD method. The CBD process involved immersing the $TiO_2$ NWA films in 20 ml solution containing 0.002 mmol $Cd(NO_3)_2$, 1 mmol thiourea and 0.02 mol $NH_3.H_2O$, and heating up to 60 □ for one hour, rinsing it thoroughly with water and drying at room temperature. The amount of QDs deposited on $TiO_2$ NWs was controlled by varying the number of CBD cycles.

The QD-SSCs were assembled by sandwiching a surlyn spacer (30 μm thick, DuPont) between the CdS quantum dot-sensitized electrode and the Pt-coated counter electrode. The space between the electrodes was filled with the polysulphide electrolyte which consisted of $Na_2S$ (0.5 M), S (0.125 M) and KCl (0.2 M), using water/methanol (7:3 by volume) solution as co-solvent.

### 2.3 Characterization

X-ray diffraction (XRD) measurement was carried out using an X-Ray Diffractometer (D-MAX 2200 VPC) with Cu Kα1 radiation. The morphology was examined by field-emission scanning electron microscopy (FESEM, JSM-6330F). The detailed microscopic characterization of CdS-coated $TiO_2$ NW was analyzed using transmission electron microscope (TEM, JEM-2010HR). Absorption spectra of samples were recorded using a spectrophotometer (Hitachi U-4100). The photocurrent-voltage (I-V) curve of each cell was measured by Keithley 2400 source meter under an illumination of a solar simulator (Newport Oriel 91192) at 100 mW $cm^{-2}$. Electron impedance spectroscopy (EIS) measurements were carried out by applying a 10 mV AC signal over the frequency range of $10^{-2}$–$10^5$ Hz under 100 mW $cm^{-2}$ illumination at open circuit voltage by using an electrochemical workstation (CHI760C).

## 3. Results and Discussion

### 3.1 XRD analysis and morphology

The phase composition of the sample was identified by XRD. As shown in Fig.1, the sample was of good crystalline nature and diffraction peaks of $TiO_2$ nanowires can be conclusively indexed as tetragonal rutile phase with the lattice constants of a=4.593 Å and c=2.959 Å, which were consistent with the values in the standard card (JCPDS 21-1276). The great enhancement of (002) diffraction peak and the absence of some diffraction peaks including (110), (111), and (211), compared to the XRD patterns of polycrystalline or powder samples, indicated that not only the highly oriented $TiO_2$ nanowires grew in the [001] direction with the growth axis perpendicular to the substrate surface, but also nanowires were single crystalline throughout their length. FESEM images of sample, as shown in Fig.2, confirmed the XRD analysis. A large-scale, highly oriented $TiO_2$ nanowires grew vertically on TCO glass substrate. The diameter of nanowires was ca. 130 nm.

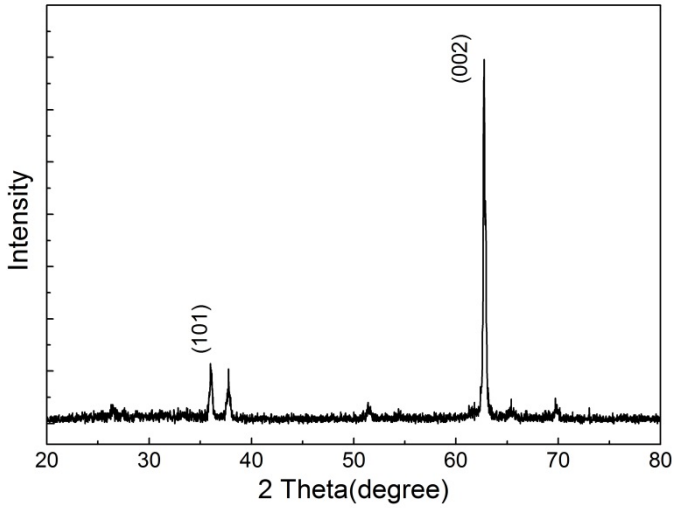


*Fig.1 XRD pattern of $TiO_2$ nanowires on TCO substrate.*

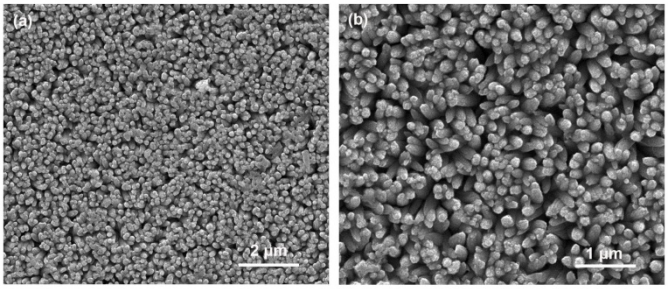


*Fig.2 SEM images of $TiO_2$ nanowire array (a) at low magnification and (b) at high magnification.*

### 3.2 Detailed microscopic characterization

High-resolution TEM (HR-TEM) and selected area electron diffraction (SAED) were used to analyze the detailed microscopic characterization of the samples. Figure 3(a) was HR-TEM image of an individual $TiO_2$ NW. The distance of 0.322 nm between the adjacent lattice fringes can be assigned to the interplanar distance of rutile $TiO_2$ (110). It was clear that the nanowire grew in the [001] direction. The well aligned spots in SAED pattern of an individual $TiO_2$ NW shown as the inset of Fig.3(a) indicated that NW was single crystalline rutile phase. These results confirmed the conclusion obtained from XRD pattern. HR-TEM image of $TiO_2$-CdS heterojunction region (Fig.3(b)) indicated the CdS modified $TiO_2$ core-shell heterostructure had been successfully

prepared. $TiO_2$ and CdS were highly crystalline. Lattice fringes with interplanar spacings, d=0.322, 0.337 nm were clearly imaged and was corresponded to the (110) planes of rutile $TiO_2$ and the (002) planes of the hexagon form of CdS respectively. The diameter of CdS nanoparticles was about in the range of 5-10 nm.

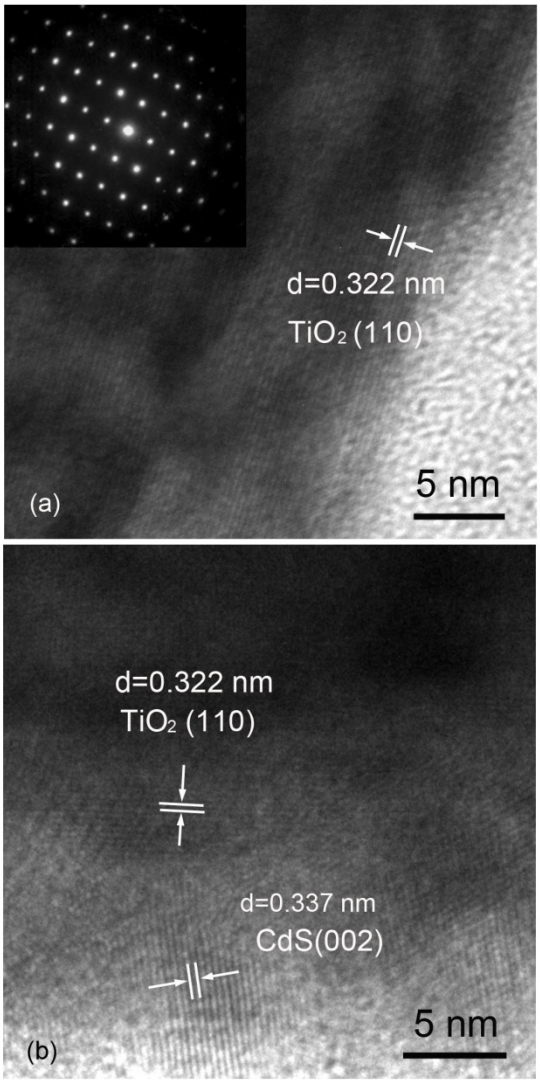


*Fig.3 (a) HR-TEM image, SAED pattern (inset) of a bare $TiO_2$ nanowire and (b) HR-TEM image of a $TiO_2$/CdS core-shell nanowire.*

### 3.3 Optical property

Fig. 4 showed the comparison of the absorption spectrum of electrodes with different number of QDs coating cycles. The CdS modification enhanced the optical absorbance of $TiO_2$ in the visible region. The absorbance intensities of electrodes increased with increasing CBD cycle number due to the increase amount of QDs deposited on the $TiO_2$ NWs films. The absorption edge of $TiO_2$-CdS(4) was approximately 515 nm obtained from the intersection of the sharply decreasing region of a spectrum with its baseline. Corresponding to this absorption edge, the band gap was calculated to be 2.41 eV. The value reported for CdS in bulk was 2.25 eV [26]. The band gap of CdS particles deposited on $TiO_2$ NWA films was higher than that of CdS bulk, which indicated that the size of the CdS particles were still within the scale of quantum dot. Estimated

from the excitonic peaks of the absorption spectra, the size of CdS particles was calculated to be ca. 5.72 nm based on the empirical equations proposed by Yu[27]. The size of CdS particles based on calculation was consistent with that observed in HR-TEM image.

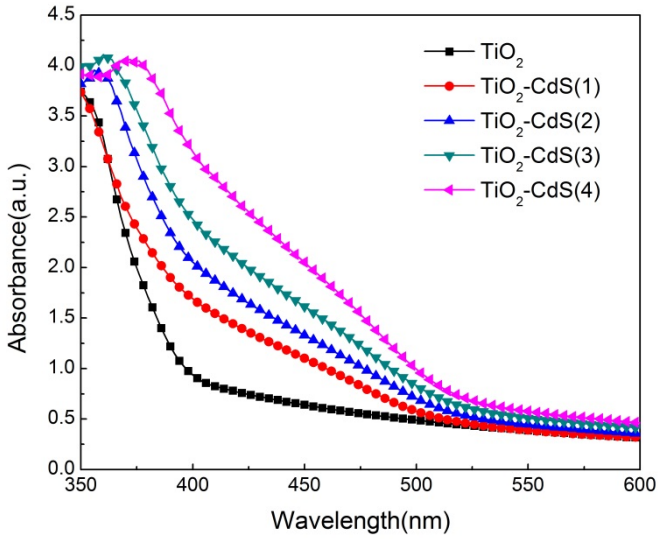


*Fig.4 UV-vis absorption spectra of bare $TiO_2$ NWA film and $TiO_2$/CdS(n) (n=1-4) electrodes.*

### 3.4 Photovoltaic performance

The number of CBD cycles introduced to prepare QD-modified films have great effect on the performance of corresponding QD-SSCs. Figure 5 showed the I-V curves of the QD-SSCs under 1.5AM, 100 mW $cm^{-2}$ illumination, the active area of cells was 0.25 $cm^2$. For the cell fabricated with bare $TiO_2$ NWs, the open circuit potential ($V_{OC}$) and the short circuit current density ($J_{SC}$) were 0.15 V and 0.34 mA $cm^{-2}$, respectively, resulting in a low energy conversion efficiency ($\eta$) of 0.016%. After CdS QDs modification, $J_{SC}$, $V_{OC}$ and $\eta$ of solar cell increased greatly, which attributed to the extending of light absorption range. $J_{SC}$ increased with the number of CdS coating cycles varying from 1 to 3 due to the increase of absorbance with increasing loading amount of CdS QDs. The QD-SSC fabricated with $TiO_2$-CdS(3) electrode exhibited the best performance, $J_{SC}$, $V_{OC}$ and $\eta$ were 7.46 mA $cm^{-2}$, 0.47 V and 1.72 %, respectively. When the number of CdS CBD cycles reached 4 or more, both $J_{SC}$ and $V_{OC}$ decreased due to the overloading of CdS QDs on the $TiO_2$ NWA film. Overloading of QDs was disadvantageous to the cell performance because the diffusion of the electrolyte was hindered by the blocking of the mesopores[28].

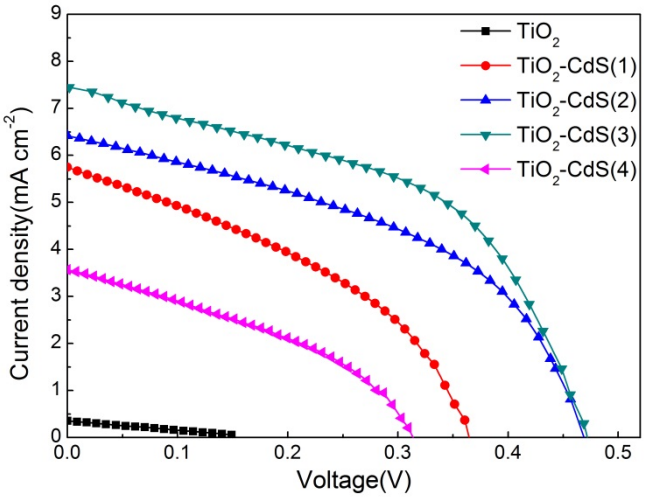


*Fig.5 Photocurrent–voltage curves of $TiO_2$ NWs based QD-SSCs measured under AM1.5 condition. The active surface area was 0.25 $cm^2$.*

### 3.5 EIS analysis

EIS measurements were carried out to investigate the kinetics of charge transfer and recombination in QD-SSCs. Figure 6 showed typical EI spectra of $TiO_2$-CdS(n)(n=0-4) based QD-SSCs measured at open circuit voltages under 1.5AM illumination. Mora-Sero´ et al.[29] have reported that when applying high forward bias at low frequency, the conductivity modulation of the electrolyte by injected electrons from the photoelectrode resulted in an inductive behavior. Thus, the impedance data obtained at different applied potentials in low-frequency range can't be fitted with a single equivalent circuit[30]. In present work, we ignored the impedance data obtained at low frequency to avoid the unnecessary interference from the inductive behavior. An equivalent circuit based on diffusion-recombination model proposed by J. Bisquert[31] used to fit the experimental data was shown as inset in Fig.6 and the fitted values were listed in Table 1. As seen from Table 1, the charge-transfer resistance related to recombination of an electron ($R_k$) decreased with the number of CdS coating cycles varying from 0 to 3, while the simulated data of the electron transfer resistance in $TiO_2$ ($R_w$) were quite similar for all cells. It is well-known that the recombination of electrons in $TiO_2$ and the hole acceptors in the electrolyte (process I) can be greatly diminished by improving QDs coverage of the $TiO_2$ surface[32]. The increasing number of CBD cycles enhanced the amount of QDs on $TiO_2$, thus blocking process I. When the CBD cycle number reached 4, the trapping of the exited electrons by the QDs' surface states (process II) and the recombination of electron in the QD conduction band and hole in the QD valence band (process III) became more important factor. Thus $R_k$ increased when CBD cycle number reached 4. The first-order reaction rate constants for the loss of electrons ($k_{eff}$) increased with the increasing amount of CdS QDs, so the electron lifetime ($\tau=1/k_{eff}$) decreased correspondingly. The effective diffusion coefficient ($D_{eff}$) can be calculated by $D_{eff}=(R_k/R_w)k_{eff}L^2$, in which $L$ represents the thickness of the $TiO_2$ film. Although $\tau$ and $D_{eff}$ decreased with the number of CBD cycles increasing from 0 to 3, $\eta$ increased. It proved that the amount of QDs was more important factor than electron lifetime and transfer rate for cell efficiency when the coverage of QDs on $TiO_2$ was not high enough. Under the combined action of process II, process III and the decrease of electron lifetime, the efficiency of $TiO_2$-CdS(4) based solar cell decreased although $D_{eff}$ increased.

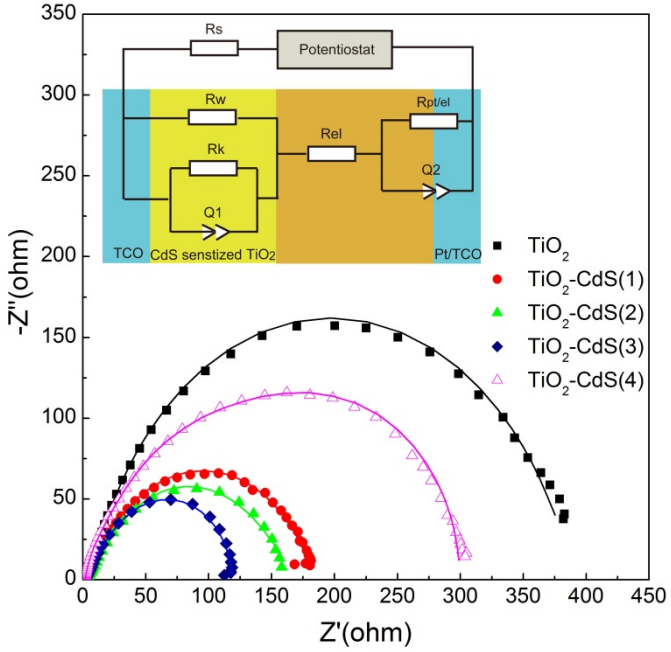


*Fig.6 Experimental (dots) and fitted (solid curve) Nyquist plots of CdS QD-SSCs under AM1.5 condition. The equivalent circuit used to fit the experimental data was shown as inset.*

*Table1 Photovoltaic performances and photoelectron transport properties of CdS QD-SSCs under AM1.5 condition*

| Sample | $V_{OC}$ (V) | $J_{SC}$ (mAcm$^{-2}$) | *FF* | $\eta$ (%) | $R_k$ (Ω) | $R_w$ (Ω) | $k_{eff}$ (s$^{-1}$) | $\tau_{eff}$ (s) | $L$ (μm) | $D_{eff}$ ×10$^5$ (cm$^2$/s) |
|---|---|---|---|---|---|---|---|---|---|---|
| Bare $TiO_2$ | 0.15 | 0.34 | 0.314 | 0.016 | 389 | 3.34 | 1.212 | 0.825 | 3.9 | 2.147 |
| $TiO_2$/CdS(1) | 0.36 | 5.75 | 0.399 | 0.825 | 182 | 3.13 | 1.778 | 0.562 | 3.9 | 1.572 |
| $TiO_2$/CdS(2) | 0.47 | 6.43 | 0.450 | 1.359 | 159 | 4.37 | 2.610 | 0.383 | 3.9 | 1.443 |
| $TiO_2$/CdS(3) | 0.47 | 7.46 | 0.490 | 1.718 | 88 | 3.23 | 2.610 | 0.383 | 3.9 | 1.081 |
| $TiO_2$/CdS(4) | 0.31 | 3.55 | 0.386 | 0.425 | 297 | 3.69 | 3.831 | 0.261 | 3.9 | 4.691 |

## 4. Conclusion

Single-crystalline $TiO_2$ nanowire arrays were grown on TCO substrates. CdS QDs were successfully assembled on $TiO_2$ NWs to obtain the $TiO_2$/CdS core-shell NW films which were used as photoanodes in solar cells. $TiO_2$/CdS heterojunction structure was confirmed by HR-TEM. A photocurrent density of 7.46 mA cm$^{-2}$, an open circuit potential of 0.47 V and a power conversion efficiency of 1.72% were achieved for the CdS QD-SSCs with the optimal CBD cycle number of 3. EIS analysis proved that the amount of QDs was more important factor than electron lifetime and transfer rate for cell efficiency when the coverage of QDs on $TiO_2$ was not high enough.

**Acknowledgment**

This work was supported by a grant from the National Natural Science Foundation of China (No. 21201047) and the Guangxi Scientific Research and Technology Development Projects (No. 11-031-08-02).

## References

[1] J. M. Maca`k, H. Tsuchiya, A. Ghicov, P. Schmuki, Electrochem. Comm. **7**, 1133 (2005).
[2] J. C. Lee, Y. M. Sung, T. G. Kim, H. J. Choi, Appl. Phys. Lett. **91**, 113104(2007).
[3] D. Kuang, J. Brillet, P. Chen, M. Takata, S. Uchida, H. Miura, K. Sumioka, S. M. Zakeeruddin, M. Gra¨ tzel, ACS NANO **2**, 1113 (2008) .
[4] X. B. Chen, S. H.Shen, L. J. Guo, S. S. Mao, Chem. Rev. **110**, 6503 (2010).
[5] J. Shi, Y. Hara, C.L. Sun, M. A. Anderson, X.D. Wang, Nano Lett. **11**, 3413 (2011).
[6] G. K. Mor, K. Shankar, M. Paulose, O. K. Varghese, C. A. Grimes, Nano Letters **6**, 215 (2006).
[7] W. Yu, L. H. Qu, W. Z. Guo, X. G. Peng, Chem. Mater. **15**, 2854 (2003).
[8] R. Vogel, P. Hoyer, H. Weller, J. Phys. Chem. B **98**, 3183 (1994).
[9] P. Wang, S. M. Zakeeruddin, J. E. Moser, R. Humphry-Baker, P. Comte, V. Aranyos, A. Hagfeldt, M. K. Nazeeruddin, M. Gratzel, Adv. Mater. **16**, 1806 (2004).
[10] C. H. Chang, Y. L. Lee, C. H. Chang, Y. L. Lee, Appl. Phys. Lett. **91**, 053503(2007).
[11] S. Kohtani, A. Kudo, T. Sakata, Chem. Phys. Lett. **206**, 166 (1993).
[12] H.J.Lee, H.C.Leventis,S.J.Moon, P. Chen, S. Ito, S. A. Haque, T. Torres, F. Nüesch, T. Geiger, S. M. Zakeeruddin, M. Grätzel, M. K. Nazeeruddin, Adv. Fun. Mater. **19**, 2735 (2009).
[13] A. Kumar, A. Jakhmola, Langmuir **28**, 2915 (2007).
[14] A. Kongkanand , K. Tvrdy , K. Takechi , M. Kuno , P. V. Kamat, J. Am. Chem. Soc. **130**, 4007 (2008).
[15] M. Li, Y. Liu, H. Wang, H. Shen, W. X. Zhao, H. Huang, C. L. Liang, J. Appl. Phys. **108**, 094304(2010).
[16] A. Zaban, O. I. Micic, B. A. Gregg, A. J. Nozik, Langmuir **14**, 3153 (1998).
[17] P. Yu , K. Zhu, A. G. Norman, S. Ferrere, A. J. Frank, A. J. Nozik, J. Phys. Chem. B **110**, 25451 (2006).
[18] A. J. Nozik, Inorg. Chem. **44**, 6893 (2005).
[19] M. Li, Y. Liu, H. Wang, W. X. Zhao, H. Huang, C. L. Liang, Y. J. Deng, H. Shen, International Journal of Photoenergy 857567(2012).
[20] M. A. Martnez, C. Guillén, J. Herrero, Applied Surface Science **136**, 8 (1998).
[21] X. Y. Yu, J. Y. Liao, K. Q. Qiu, D. B. Kuang, C. Y. Su, ACS NANO **5**, 9494 (2011).
[22] L. Claude, C. Ramon, T. M. Ryan, Adv. Mater. **17**, 1512 (2005).
[23] J. C. Lee, T. G. Kim, H. J. Choi, Y. M. Sung, Crystal Growth &Design **7**, 2588 (2007).
[24] M. E. Rincon, O. Gomez-Daza, C. Corripio, A. Orihuela, Thin Solid Films **389**, 91 (2001).
[25] B. Liu and E. S. Aydil, J. Am. Chem. Soc. **131**, 3985 (2009).
[26] Y. L. Lee and Y. S. Lo, Advanced Functional Materials **19**, 604 (2009).
[27] W. W. Yu, L. H. Qu, W. Z. Guo and X. G. Peng, Chem. Mater. **15**, 2854 (2003).
[28] P. Sudhagar, J. H. Jung, S. Park, Y. G. Lee, R. Sathyamoorthy, Y. S. Kang H. Ahn,

Electrochem. Comm. **11**, 2220 (2009).
[29] I. Mora-Seró , J. Bisquert , F.Fabregat-Santiago , G. Garcia-Belmonte, Nano Lett. **6**, 640 (2006).
[30] H. M. Cheng, W. H. Chiu, C. H. Lee, S. Y. Tsai, W. F. Hsieh, J. Phys. Chem. C **112**, 16359 (2008).
[31] J. Bisquert, J. Phys. Chem. B **106**, 325 (2002).
[32] X.Y. Yu, J.Y. Liao, K.Q. Qiu, D.B. Kuang, C.Y. Su, ACS NANO **5**, 94940(2011).